

Article 17 of your GA provides details on the acknowledgments. For your convenience, I indicate below how this should be phrased:

For publications: “Funded by the European Union” or “Funded by the European Union under grant agreement No [number]”

## $^1\text{H}$ , $^{13}\text{C}$ and $^{15}\text{N}$ chemical shift assignments of Rubella virus macro domain in the free and in the ADPr bound state

Danai Moschidi<sup>1</sup>, Nikolaos K. Fourkiotis<sup>1</sup>, Christos Sideras-Bisdekis<sup>1</sup>, Aikaterini C. Tsika<sup>1</sup>, Georgios A. Spyroulias<sup>1\*</sup>

<sup>1</sup> *Department of Pharmacy, University of Patras, 26504 Patras, Greece*

\*to whom correspondence should be addressed: [ktsika@upatras.gr](mailto:ktsika@upatras.gr), [G.A.Spyroulias@upatras.gr](mailto:G.A.Spyroulias@upatras.gr)

D. Moschidi and N. K. Fourkiotis contributed equally

## Keywords

Rubella virus (RuV); Macro domain (MD); ADP-ribosylation; Solution NMR spectroscopy

## Abstract

Prokaryotes, eukaryotes and certain viruses with positive single-stranded RNA genomes are among the forms of life that have been found to possess macro domains (MDs). There are claims that viral MDs inhibit the immune response mediated by PARPs, such as PARP12 and PARP14, and are involved in the formation of the viral replication transcription complex (RTC). Rubella virus (RuV) is included in this group of viruses. Its MD acts as an “eraser” of the post translation modification (PTM) ADP-ribosylation by binding to and hydrolyzing ADP-ribose (ADPr) from ADP-ribosylated substrates including proteins and nucleic acids. Consequently, it represents an attractive pharmacological target. Currently, no inhibitors exist for RuV MD's de-ADP-ribosylation activity, which may play a crucial role in viral replication and pathogenesis, as observed in severe acute respiratory syndrome coronavirus (SARS-CoV) and Chikungunya virus (CHIKV). RuV remains a serious threat, particularly to unvaccinated children, with approximately 10,000 of the 18,000 global cases in 2022 reported in Africa. Alarmingly, no FDA-approved drugs are available for RuV treatment. In this study, we present the almost complete NMR backbone and side-chain resonance assignment of RuV MD in both free and ADPr bound form, along with the NMR chemical shift-based secondary structure element prediction. These findings will support the efficient screening of fragments or chemical libraries using NMR spectroscopy to identify compounds that are strong binders and potentially exhibit antiviral activity.

## Biological context

Rubella virus (RuV) belongs to the *Matonaviridae* family and the genus *Rubivirus*, which includes two other viruses that infect only animals, the Ruhugu virus (RuhV) found in bats and the Rustrela virus (RusV) in rodents (Bennett *et al.*, 2020; Mankertz *et al.*, 2022). The symptoms of Rubella, a highly contagious virus that spreads through droplets, include fever, coughing, while sometimes the patients also develop arthritis, painful joints and a rash (Kilich, Perelygina and Sullivan, 2024). Even though there is a safe and cost-effective vaccine which protects against Rubella, there were reported approximately 18,000 cases of Rubella worldwide in 2022 according to the World Health Organization (WHO) ([WHO], 2024). Rubella is regarded as one of the world's most common causes of death for children. It can also infect pregnant women during the first trimester, potentially causing fetal death or resulting in babies with congenital rubella syndrome (CRS) ([WHO], 2024). *Matonaviridae* family consists of enveloped viruses that possess single-stranded positive-sense RNA genome ((+)ssRNA) of up to 10 kb in length and high in GC content, with RuV having (+)ssRNA close to 9.6 kb and 69%, respectively. RuV genome encodes three structural proteins from its 3'ORF, the capsid (C) and the two glycoproteins E1 and E2, and one non-structural protein (nsP) named p200 from its 5'ORF. p200 is further processed into two nsPs, the p90 and the p150 (Matthews, Tzeng and Frey, 2010), that are vital for the formation of replication transcription complex (Marr, Wang and Frey, 1994). p90 consists of two protein domains, the helicase (Hel) and the RNA-dependent RNA polymerase (RdRp), while p150 contains three independent domains, the methyltransferase (MTase), the macro domain (MD) and the papain-like protease (PLpro) (Prasad *et al.*, 2013; Cheong *et al.*, 2022). Other (+)ssRNA viruses belonging to viral families, such as *Togaviridae*, *Coronaviridae* and *Hepeviridae*, also possess MDs (Makrynitsa *et al.*, 2015; Melekis *et al.*, 2015; Li *et al.*, 2016; Lykouras *et al.*, 2018; Grunewald *et al.*, 2019; Palazzo *et al.*, 2019; Tsika *et al.*, 2019, 2022; Leung *et al.*, 2022; Politi *et al.*, 2023). The MDs exhibit the  $\alpha/\beta/\alpha$  three-layered sandwich structure (Tsika *et al.*, 2019), comprised of several Rossmann  $\beta$ - $\alpha$ - $\beta$  motifs. These secondary structure elements are assembled in a central mixed  $\beta$ -sheet, consisting of 6-7  $\beta$ -strands flanked by 4-5  $\alpha$ -helices, forming on one side of the molecule a positively charged cavity that is responsible for binding ADPr, nucleic acids and other NAD<sup>+</sup>

derivatives (Cantini *et al.*, 2020; Fourkiotis *et al.*, 2022; Tsika, *et al.*, 2022). Moreover, the structure of MDs closely resembles the structure of proteins that bind NAD<sup>+</sup> derivatives-nucleic acids, such as leucine aminopeptidases (Allen *et al.*, 2003). Today, many MD structures for a variety of organisms, either in their free or bound to ADPr or other small molecules form, have been solved (Malet *et al.*, 2009; Forst *et al.*, 2013; Cho *et al.*, 2016; Tsika *et al.*, 2019; Michalska *et al.*, 2020). This is also the case for Rubella virus, as the structures of RuV MD, both in free and ADPr bound state, have been recently solved through X-ray crystallography (Stoll *et al.*, 2024). RuV MD structure resembles that of other viral MD domains in the MacroD-type family, such as the MD of Mayaro virus (MAYV) (Tsika *et al.*, 2019) and SARS-CoV-2 (Alhammad *et al.*, 2021), which belong to Alphaviruses and Coronaviruses, respectively (Stoll *et al.*, 2024). Note that the RuV MD exhibits higher sequence identity with Alphaviruses MD than with Coronaviruses MD. It has the highest sequence identity to MAYV MD (32%) and the lowest to SARS-CoV MD (24%) (Fig. 1).

Regarding its activity, it was shown that RuV MD possesses the capacity to remove either single ADPr units (MAR) or ADPr chains (PAR), from substrates that have been ADP-ribosylated; these characteristics are also known as de-MARylation and de-PARylation, respectively, and the first is a feature of most of the viral MDs (Stoll *et al.*, 2024). Viral MDs ability to bind ADPr, its derivatives (e.g. PAR, OAADPr) and nucleic acids were initially not associated with any biological function, until the de-MARylation activity of Hepatitis E virus (HEV) was discovered (Li *et al.*, 2016). In recent years, their dual role as “readers” and “erasers” of ADP-ribosylation, *in vitro* and *in vivo*, has made them molecules of particular biological and medicinal interest (Fehr *et al.*, 2016; Alhammad *et al.*, 2023). Following infection by (+)ssRNA viruses, host cells enhance PARP-mediated ADP-ribosylation, whereas viral macro domains counteract this modification, potentially allowing the virus to evade antiviral defenses. As an example, PARP10 targets and MARYlates the protease of CHIKV, rendering it inactive, while CHIKV reverses this PTM through its MD, by hydrolytically removing MAR (Krieg *et al.*, 2023). This could be the case for more viral and/or host proteins in the context of antiviral response (Li *et al.*, 2016; Alhammad and Fehr, 2020; Fourkiotis *et al.*, 2022). The fact that viral MDs capability of removing MAR from their substrates enhances their pathogenicity was supplemented by the discovery that their ability to

simply bind free or bound to substrate ADPr affects the replication process of the viral genome (Abraham *et al.*, 2020; Voth *et al.*, 2021; Kerr *et al.*, 2024). So, viral MDs like RuV MD are considered potential drug targets, and work is being performed to find new molecules that can inhibit their function (Berg *et al.*, 2022).

The almost complete RuV MD backbone and side-chain resonance assignment is presented here in both free and ADPr bound forms. Even though the structures of RuV MDs in the free (PDB ID: 8P0C) and ADPr bound state (PDB ID: 8P0E) have previously been solved by X-ray Crystallography, NMR study provides important insights into the protein's dynamics and allows the characterization of biomolecular interactions with potential ligands in a setting that is similar to its native *in vivo* environment.

## Methods and experiments

### Construct design

A codon optimized gene (Uniprot accession number: Q99IE5) encoding the RuV MD (806-985 a.a., which is part of the protease/methyltransferase p150 polypeptide of the non-structural polyprotein p200) for expression in the heterologous system *E.coli* was obtained from GenScript (Piscataway, NJ). It was amplified with PCR and cloned into pET20b(+) expression vector between the restriction sites *NdeI-XhoI*. The polypeptide was expressed with cloning artifact amino acids, one at the N-terminal region (Methionine) and two, Leucine and Glutamate, preceding the uncleavable His<sub>6</sub>-tag in the C-terminus. For the verification of the obtained construct DNA sequencing was used.

### Protein expression and uniform <sup>15</sup>N and <sup>15</sup>N/<sup>13</sup>C labeling

The plasmid expressing RuV MD was transformed into Rosetta<sup>TM</sup>2(DE3) pLysS *E. coli* cells. A *Luria-Bertani* (LB) pre-culture that was inoculated with the above cells was grown overnight at 37 °C with shaking at 180 rpm. This pre-culture was then used to inoculate a 0.5 L M9 minimal medium (40 mM Na<sub>2</sub>HPO<sub>4</sub>, 22 mM KH<sub>2</sub>PO<sub>4</sub>, 8 mM NaCl) containing 0.5 g <sup>15</sup>NH<sub>4</sub>Cl and 2 g unlabeled or <sup>13</sup>C-D-glucose, 1 mL from a stock solution containing 0.5 mg/mL biotin and 0.5 mg/mL thiamine, 0.5

mL of 1 M Mg<sub>2</sub>SO<sub>4</sub>, 0.15 mL of 1 M CaCl<sub>2</sub>, 1 mL of trace elements solution (40 mM HCl, 50 mg/L FeCl<sub>2</sub>·4H<sub>2</sub>O, 184 mg/L CaCl<sub>2</sub>·2H<sub>2</sub>O, 64 mg/L H<sub>3</sub>BO<sub>3</sub>, 18 mg/L CoCl<sub>2</sub>·6H<sub>2</sub>O, 4 mg/L CuCl<sub>2</sub>·2H<sub>2</sub>O, 340 mg/L ZnCl<sub>2</sub>, 710 mg/L Na<sub>2</sub>MoO<sub>4</sub>·2H<sub>2</sub>O, 40 mg/L MnCl<sub>2</sub>·4H<sub>2</sub>O), 0.5 mL of 10X stock solution of BioExpress® 1000 (U-<sup>13</sup>C, 98%; U-<sup>15</sup>N, 98%), 100 µg/mL ampicillin and 34 µg/mL chloramphenicol. The culture was incubated at 37 °C with shaking at 180 rpm until the OD<sub>600</sub> was between 0.6-0.8 and adaptation at 18 °C followed for 2 h. IPTG to final concentration of 1 mM was added to the culture, which finally was incubated overnight at 18 °C with shaking at 180 rpm.

### **Protein purification and sample preparation**

For the purification of the MD of RuV, the cells were harvested by centrifugation that was performed at 4 °C and at 8,000 rpm for 10 min (Thermo Scientific®, Sorvall Lynx 6000). Then, the cell pellet was resuspended with 25 mL lysis buffer (10 mM Imidazole, 50 mM Tris pH 8, 500 mM NaCl) and 10 µL of protease inhibitor cocktail (Sigma Aldrich® P8849), 10% glycerol and 2 mM DTT. After the resuspended cells were sonicated (PMisonix®, Sonicator 4000), 50 µL DNase (1.6 mg/mL) were added to the suspension, which was further incubated for 10 min on ice. The cell extract was centrifuged at 4 °C at 14,000 rpm for 30 min. The soluble fraction containing the His<sub>6</sub>-tagged RuV MD was filtrated with 0.22 µm membrane filter and was loaded onto a 5 mL HisTrap™FF affinity column (Cytiva) that had been previously equilibrated with 0.1 M NiSO<sub>4</sub>·6H<sub>2</sub>O and 5 column volumes (CV) lysis buffer. The protein was eluted using a step gradient with increasing concentration of imidazole (10, 20, 40, 100, 200, 400 mM imidazole in buffer containing also 50 mM Tris pH 8, 500 mM NaCl). RuV MD eluted mostly in 100 and 200 mM imidazole-containing buffers. Using an Amicon® Ultra 15 mL Centrifugal Filter membrane (nominal molecular weight cutoff 10 kDa), the protein was concentrated to final volume of 1 mL, and as well buffer exchange was performed from the imidazole-containing buffer to NMR buffer containing 50 mM NaPi pH 7.6, 50 mM NaCl, 2 mM EDTA, 2 mM DTT. The concentrated protein sample was then loaded to a Superdex 75 10/300 GL (GE Healthcare) column, previously equilibrated with NMR buffer, to remove any impurities. The elution fractions were analyzed by SDS-PAGE (17%) and Coomassie staining and the ones containing the pure protein were pooled together and concentrated to final volume of 500 µL. The final NMR samples had a final volume

of 552  $\mu\text{L}$  and were prepared by adding 1  $\mu\text{L}$  of proteases inhibitor cocktail (Sigma Aldrich<sup>®</sup> P8849), 10%  $\text{D}_2\text{O}$  and 0.25 mM DSS (4,4-dimethyl-4-silapentane-1-sulfonic acid - Sigma Aldrich<sup>®</sup>) used as internal  $^1\text{H}$  chemical shift standard. Apart from the RuV MD apo state, the ADPr bound state in molar ratio of RuV MD:ADPr - 1:5 (Sigma Aldrich<sup>®</sup>) was studied. The concentration of the double labeled  $^{15}\text{N}$ ,  $^{13}\text{C}$  RuV MD samples was 0.82 mM for the free form and 0.62 mM for the ADPr bound form while the  $^{15}\text{N}$  RuV MD samples were at 0.6 mM for the free form and at 0.45 mM for the ADPr bound form.

### **NMR data acquisition and processing**

All NMR experiments were recorded at 298 K on a Bruker Avance III High-Definition four-channel 700 MHz NMR spectrometer equipped with a cryogenically cooled 5 mm  $^1\text{H}/^{13}\text{C}/^{15}\text{N}/\text{D}$  Z-gradient probe (TCI). Table 1 provides an overview of the NMR experiments and corresponding main parameters acquired for backbone and side-chain assignments for both free and ADPr bound form. The assignments of RuV MD in both states were obtained through analyzing the subsequent set of heteronuclear experiments: 2D  $^1\text{H},^{15}\text{N}$  HSQC and 2D  $^1\text{H},^{13}\text{C}$  HSQC, 3D HN(CO)CA, 3D HNCA, 3D HN(CO)CACB, 3D HNCACB, 3D HN(CA)CO, 3D HNCO, 3D HNHA, 3D HBHA(CBCACO)NH, 3D aliphatic (H)CCH–TOCSY and 3D  $^1\text{H},^{15}\text{N}$  NOESY, 3D  $^1\text{H},^{13}\text{C}$  aliphatic NOESY and 3D  $^1\text{H},^{13}\text{C}$  aromatic NOESY. All NMR data were processed using TopSpin 3.7.0 (Bruker Biospin) and analyzed using CARA 1.9.1.7 (Keller, 2004).

### **Extent of assignments and data deposition**

In both free (Fig. 2a) and ADPr bound (Fig. 2b) forms, the amide signals in the 2D  $^1\text{H},^{15}\text{N}$  HSQC spectra are well-dispersed, which is a sign of a well-folded protein in absence and presence of ADPr. For the RuV MD apo, 92% of  $^1\text{H}^{\text{N}}/^{15}\text{N}$  backbone pairs, 93% of  $^{13}\text{CO}$ , 94% of  $^{13}\text{C}\alpha$  and 94% of  $^{13}\text{C}\beta$  chemical shifts as well 69% of the total atoms of side chains of native protein sequence (806-985 a.a.) were assigned. Regarding the ADPr bound form, 84% of the  $^1\text{H}^{\text{N}}/^{15}\text{N}$  backbone pairs, 87% of  $^{13}\text{CO}$ , 88% of  $^{13}\text{C}\alpha$  and 88% of  $^{13}\text{C}\beta$  chemical shifts as well 65% of the total atoms of side chains of native protein sequence were assigned. The unassigned residues in 2D  $^1\text{H},^{15}\text{N}$  HSQC

spectrum of RuV MD in the apo form, except for the 13 prolines present in the sequence, correspond to the residues S806 to D807, G832, K834, S848 to V850, A861, R900, V940, Y941, D972 to A974 and the His<sub>6</sub>-tag. In the ADPr bound form, apart from the unassigned residues in apo form with the exception of R973-A974, the residues D825-I826, A839 to E842, G847 to F855, A895 and L935-L936 were also not assigned. These residues are in the loops of RuV MD which are mainly forming the binding site of ADPr. Specifically, the residues D825-I826 located in the  $\beta$ 2- $\beta$ 3 loop, that are conserved in most viral macro domains and are responsible for the stabilization of the adenine group of ADPr, disappeared in the presence of ADPr (Fig. 3b). Moreover, the residues at the end of  $\beta$ 3 and the catalytic loop  $\beta$ 3- $\alpha$ 1, A839 to E842, as well the residues G847 to F855 located in  $\alpha$ 1, which interact with the distal ribose of ADPr, are broadened beyond detection upon ADPr binding (Fig. 3b). Furthermore, the residues V940-Y941 located in the  $\beta$ 6- $\alpha$ 4 loop that bind the phosphate groups of ADPr were not assigned in both apo and bound states while the residues L935-L936 located in the same loop disappeared with the ADPr addition (Fig. 3b). The appearance and disappearance of the signals in the ADPr bound form suggests conformational exchange in these regions to accommodate the ligand. Similar observations were made in the NMR studies of a human MD belonging to hPARP14 and of the coronaviruses' MDs from SARS-CoV and SARS-CoV-2 (Cantini et al., 2020; Fourkiotis et al., 2022; Tsika et al., 2022). In contrast, for the MD of alphavirus MAYV, the opposite effect took place, the structure upon ADPr binding became more rigid and these conserved residues were observable, which was not true for the apo state (Tsika *et al.*, 2019).

The secondary structure prediction for both apo and ADPr bound forms was achieved based on the chemical shift assignments of the backbone atoms <sup>1</sup>H<sup>N</sup>, <sup>15</sup>N, <sup>13</sup>CO, <sup>13</sup>C $\alpha$ , <sup>1</sup>H $\alpha$  and <sup>13</sup>C $\beta$  using the TALOS+ server (Shen *et al.*, 2009). Both forms adopt a  $\alpha/\beta/\alpha$  three layered sandwich fold, consisting of 7 beta strands and 5 alpha helices with  $\beta/\beta/\beta/\alpha/\alpha/\beta/\beta/\alpha/\beta/\alpha/\beta/\alpha$  topology (Fig. 4), typical for the macro domain fold, with no significant differences between the two states. Moreover, the resulting secondary elements were compared with the existing crystal structures of the RuV MD (apo form PDB ID: 8POC and bound form PDB ID: 8POE) (Stoll *et al.*, 2024) and they are in good agreement as shown in Fig. 4. The flexibility of RuV MD in apo and ADPr bound state was also predicted and described as Random Coil Index (RCI) derived S<sup>2</sup> values (RCI-S<sup>2</sup>) (blue dots

in Fig. 4). Most RCI-S<sup>2</sup> values are close to 1, a sign of a rigid structure, except for the N- and C-termini and the loops in which the values are lower, a sign of more flexible regions.

All the chemical shift data of RuV MD in both free and ADPr bound forms have been deposited in the Biological Magnetic Resonance Bank (<https://bmrbl.io>) under accession numbers 52869 and 52870, respectively.

**Acknowledgements** Open access funding provided by HEAL-Link Greece. This work is partially funded by the European Union programs HORIZON-WIDERA-2022-TALENTS-01 ERA Chairs “ESPERANCE” project under grant agreement No GA 101087215 (DOI: 10.3030/101087215; to DM, NKF, ACT & GAS) and HORIZON-WIDERA-2023-ACCESS-04 Pathways to Synergies “MILESTONE” project under grant agreement No GA 101159708 (DOI: 10.3030/101159708; to CSB & GAS). We also acknowledge EU FP7 REGPOT CT-2011–285950—“SEE-DRUG” project for the purchase of UPAT’s 700 MHz NMR equipment.

**Author contributions** DM data analysis, writing & manuscript editing. NKF protein expression and purification, writing & manuscript editing. CSB protein expression and purification, writing & manuscript editing. ACT protein expression and purification, conceptualization, methodology, supervision, writing & manuscript editing. GAS conceptualization, data acquisition, writing & manuscript editing, supervision, funding acquisition, project administration & management, resources.

**Data availability** All the chemical shift values of RuV MD apo and ADPr bound forms were deposited in the Biological Magnetic Resonance Data Bank (BMRB) under accession numbers 52869 and 52870, respectively.

## **Conflict of Interest**

The authors declare no conflict of interest.

## References

Abraham, R. *et al.* (2020) 'Both ADP-ribosyl-binding and hydrolase activities of the alphavirus nsp3 macrodomain affect neurovirulence in mice', *mBio*, 11(1). Available at: <https://doi.org/10.1128/mBio.03253-19>.

Alhammad, Y.M. *et al.* (2023) 'SARS-CoV-2 Mac1 is required for IFN antagonism and efficient virus replication in cell culture and in mice', *Proceedings of the National Academy of Sciences of the United States of America*, 120(35). Available at: <https://doi.org/10.1073/pnas.2302083120>.

Alhammad, Y.M.O. and Fehr, A.R. (2020) 'The viral macrodomain counters host antiviral ADP-ribosylation', *Viruses*. MDPI AG. Available at: <https://doi.org/10.3390/v12040384>.

Allen, M.D. *et al.* (2003) 'The crystal structure of AF1521 a protein from *Archaeoglobus fulgidus* with homology to the non-histone domain of macroH2A', *Journal of Molecular Biology*, 330(3), pp. 503–511. Available at: [https://doi.org/10.1016/S0022-2836\(03\)00473-X](https://doi.org/10.1016/S0022-2836(03)00473-X).

Bennett, A.J. *et al.* (2020) 'Relatives of rubella virus in diverse mammals', *Nature*, 586(7829), pp. 424–428. Available at: <https://doi.org/10.1038/s41586-020-2812-9>.

Berg, H. *et al.* (2022) 'Comprehensive Fragment Screening of the SARS-CoV-2 Proteome Explores Novel Chemical Space for Drug Development', *Angewandte Chemie - International Edition*, 61(46). Available at: <https://doi.org/10.1002/anie.202205858>.

Cantini, F. *et al.* (2020) '1H, 13C, and 15N backbone chemical shift assignments of the apo and the ADP-ribose bound forms of the macrodomain of SARS-CoV-2 non-structural protein 3b', *Biomolecular NMR Assignments*, 14(2), pp. 339–346. Available at: <https://doi.org/10.1007/s12104-020-09973-4>.

Cheong, E.Z.K. *et al.* (2022) 'Crystal structure of the Rubella virus protease reveals a unique papain-like protease fold', *Journal of Biological Chemistry*, 298(8). Available at: <https://doi.org/10.1016/j.jbc.2022.102250>.

Cho, C.C. *et al.* (2016) 'Macro domain from middle east respiratory syndrome coronavirus (MERS-CoV) is an efficient ADP-ribose binding module: Crystal structure and biochemical studies', *Journal of Biological Chemistry*, 291(10), pp. 4894–4902. Available at: <https://doi.org/10.1074/jbc.M115.700542>.

Fehr, A.R. *et al.* (2016) 'The conserved coronavirus macrodomain promotes virulence and suppresses the innate immune response during severe acute respiratory syndrome coronavirus infection', *mBio*, 7(6). Available at: <https://doi.org/10.1128/mBio.01721-16>.

Forst, A.H. *et al.* (2013) 'Recognition of mono-ADP-ribosylated ARTD10 substrates by ARTD8 macrodomains', *Structure*, 21(3), pp. 462–475. Available at: <https://doi.org/10.1016/j.str.2012.12.019>.

Fourkotis, N.K. *et al.* (2022) 'NMR study of human macroPARPs domains: 1H, 15N and 13C resonance assignment of hPARP14 macro domain 2 in the free and the ADPr bound state', *Biomolecular NMR Assignments*, 16(2), pp. 399–406. Available at: <https://doi.org/10.1007/s12104-022-10110-6>.

Grunewald, M.E. *et al.* (2019) 'The coronavirus macrodomain is required to prevent PARP-mediated inhibition of virus replication and enhancement of IFN expression', *PLoS Pathogens*, 15(5). Available at: <https://doi.org/10.1371/journal.ppat.1007756>.

Keller, R.L.J. (2004) *The Computer Aided Resonance Assignment Tutorial*.

Kerr, C.M. *et al.* (2024) 'Mutation of a highly conserved isoleucine residue in loop 2 of several SARS-CoV-2 coronavirus macrodomains indicates that enhanced ADP-ribose binding is detrimental to infection'. Available at: <https://doi.org/10.1101/2024.01.03.574082>.

Kilich, G., Perelygina, L. and Sullivan, K.E. (2024) 'Rubella virus chronic inflammatory disease and other unusual viral phenotypes in inborn errors of immunity', *Immunological Reviews*. John Wiley and Sons Inc, pp. 113–137. Available at: <https://doi.org/10.1111/imr.13290>.

Krieg, S. *et al.* (2023) 'Mono-ADP-ribosylation by PARP10 inhibits Chikungunya virus nsP2 proteolytic activity and viral replication', *Cellular and Molecular Life Sciences*, 80(3). Available at: <https://doi.org/10.1007/s00018-023-04717-8>.

Leung, A.K.L. *et al.* (2022) 'The Conserved Macrodomain Is a Potential Therapeutic Target for Coronaviruses and Alphaviruses', *Pathogens*, 11(1). Available at: <https://doi.org/10.3390/pathogens11010094>.

Li, C. *et al.* (2016) 'Viral Macro Domains Reverse Protein ADP-Ribosylation', *Journal of Virology*, 90(19), pp. 8478–8486. Available at: <https://doi.org/10.1128/jvi.00705-16>.

Lykouras, M. V. *et al.* (2018) 'NMR study of non-structural proteins—part III: <sup>1</sup>H, <sup>13</sup>C, <sup>15</sup>N backbone and side-chain resonance assignment of macro domain from Chikungunya virus (CHIKV)', *Biomolecular NMR Assignments*, 12(1), pp. 31–35. Available at: <https://doi.org/10.1007/s12104-017-9775-2>.

Makrynitsa, G.I. *et al.* (2015) 'NMR study of non-structural proteins—part II: <sup>1</sup>H, <sup>13</sup>C, <sup>15</sup>N backbone and side-chain resonance assignment of macro domain from Venezuelan equine encephalitis virus (VEEV)', *Biomolecular NMR Assignments*, 9(2), pp. 247–251. Available at: <https://doi.org/10.1007/s12104-014-9584-9>.

Malet, H. *et al.* (2009) 'The Crystal Structures of Chikungunya and Venezuelan Equine Encephalitis Virus nsP3 Macro Domains Define a Conserved Adenosine Binding Pocket', *Journal of Virology*, 83(13), pp. 6534–6545. Available at: <https://doi.org/10.1128/jvi.00189-09>.

Mankertz, A. *et al.* (2022) 'ICTV Virus Taxonomy Profile: Matonaviridae 2022', *Journal of General Virology*, 103(12). Available at: <https://doi.org/10.1099/jgv.0.001817>.

Marr, L.D., Wang, C.Y. and Frey, T.K. (1994) 'Expression of the Rubella Virus Nonstructural Protein ORF and Demonstration of Proteolytic Processing', *Virology*, 198(2), pp. 586–592. Available at: <https://doi.org/10.1006/VIRO.1994.1070>.

Matthews, J.D., Tzeng, W.P. and Frey, T.K. (2010) 'Analysis of the function of cytoplasmic fibers formed by the rubella virus nonstructural replicase proteins', *Virology*, 406(2), pp. 212–227. Available at: <https://doi.org/10.1016/j.virol.2010.07.025>.

- Melekis, E. *et al.* (2015) 'NMR study of non-structural proteins—part I: <sup>1</sup>H, <sup>13</sup>C, <sup>15</sup>N backbone and side-chain resonance assignment of macro domain from Mayaro virus (MAYV)', *Biomolecular NMR Assignments*, 9(1), pp. 191–195. Available at: <https://doi.org/10.1007/s12104-014-9572-0>.
- Michalska, K. *et al.* (2020) 'Crystal structures of SARS-CoV-2 ADP-ribose phosphatase: From the apo form to ligand complexes', *IUCr*, 7, pp. 814–824. Available at: <https://doi.org/10.1107/S2052252520009653>.
- Palazzo, L. *et al.* (2019) 'ADP-ribosylation signalling and human disease', *Open Biology*. Royal Society Publishing. Available at: <https://doi.org/10.1098/rsob.190041>.
- Politi, M.D. *et al.* (2023) '<sup>1</sup>H, <sup>13</sup>C, <sup>15</sup>N backbone resonance assignment of apo and ADP-ribose bound forms of the macro domain of Hepatitis E virus through solution NMR spectroscopy', *Biomolecular NMR Assignments*, 17(1), pp. 1–8. Available at: <https://doi.org/10.1007/s12104-022-10111-5>.
- Prasad, V.M. *et al.* (2013) 'Rubella virus capsid protein structure and its role in virus assembly and infection', *Proceedings of the National Academy of Sciences of the United States of America*, 110(50), pp. 20105–20110. Available at: <https://doi.org/10.1073/pnas.1316681110>.
- Shen, Y. *et al.* (2009) 'TALOS+: A hybrid method for predicting protein backbone torsion angles from NMR chemical shifts', *Journal of Biomolecular NMR*, 44(4), pp. 213–223. Available at: <https://doi.org/10.1007/s10858-009-9333-z>.
- Stoll, G.A. *et al.* (2024) 'Crystal structure and biochemical activity of the macrodomain from rubella virus p150', *Journal of Virology*, 98(2). Available at: <https://doi.org/10.1128/jvi.01777-23>.
- Tsika, A.C. *et al.* (2019) 'Deciphering the Nucleotide and RNA Binding Selectivity of the Mayaro Virus Macro Domain', *Journal of Molecular Biology*, 431(12), pp. 2283–2297. Available at: <https://doi.org/10.1016/j.jmb.2019.04.013>.
- Tsika, A.C. *et al.* (2022) 'NMR study of macro domains (MDs) from betacoronavirus: backbone resonance assignments of SARS-CoV and MERS-CoV MDs in the free and the ADPr-bound state', *Biomolecular NMR Assignments*, 16(1), pp. 9–16. Available at: <https://doi.org/10.1007/s12104-021-10052-5>.
- Voth, L.S. *et al.* (2021) 'Unique Mutations in the Murine Hepatitis Virus Macrodomain Differentially Attenuate Virus Replication, Indicating Multiple Roles for the Macrodomain in Coronavirus Replication', *Journal of Virology*, 95(15). Available at: <https://doi.org/10.1128/jvi.00766-21>.
- World Health Organization. (2024). Rubella fact sheet. Retrieved from <https://www.who.int/news-room/fact-sheets/detail/rubella>

## Table

**Table 1.** List of NMR experiments acquired at 700 MHz spectrometer at 298 K and corresponding main parameters used for backbone and side-chain assignments for RuV apo (a) and ADPr bound (b) form.

	Time domain data size (points)			Spectral width/Carrier frequency (ppm)			NS	Delay time (s)
	t1	t2	t3	F1	F2	F3		
<b>(a) RuV apo</b>								
<sup>1</sup> H, <sup>15</sup> N HSQC	256	2048		44/120 ( <sup>15</sup> N)	14/4.7 ( <sup>1</sup> H)		4	1
<sup>1</sup> H, <sup>13</sup> C HSQC	512	2048		160/80 ( <sup>13</sup> C)	14/4.7 ( <sup>1</sup> H)		32	1
CBCANH	96	40	1024	72/39 ( <sup>13</sup> C)	44/117 ( <sup>15</sup> N)	14/4.7 ( <sup>1</sup> H)	32	1
CBCA(CO)NH	96	40	1024	72/39 ( <sup>13</sup> C)	44/117 ( <sup>15</sup> N)	14/4.7 ( <sup>1</sup> H)	32	1
HNCA	80	40	1024	42/55 ( <sup>13</sup> C)	44/117 ( <sup>15</sup> N)	14/4.7 ( <sup>1</sup> H)	8	1
HN(CO)CA	80	40	1024	42/55 ( <sup>13</sup> C)	44/117 ( <sup>15</sup> N)	14/4.7 ( <sup>1</sup> H)	16	1
HNCO	64	40	1024	18/175 ( <sup>13</sup> C)	44/117 ( <sup>15</sup> N)	14/4.7 ( <sup>1</sup> H)	8	1
HN(CA)CO	64	40	1024	18/175 ( <sup>13</sup> C)	44/117 ( <sup>15</sup> N)	14/4.7 ( <sup>1</sup> H)	8	1
HNHA	48	96	1024	35/117 ( <sup>15</sup> N)	14/4.7 ( <sup>1</sup> H)	14/4.7 ( <sup>1</sup> H)	16	1
HBHA(CBCACO)NH	112	40	1024	8/4.7 ( <sup>1</sup> H)	44/117 ( <sup>15</sup> N)	14/4.7 ( <sup>1</sup> H)	16	1
(H)CCH-TOCSY	128	48	1024	80/39 ( <sup>13</sup> C)	80/39 ( <sup>13</sup> C)	14/4.7 ( <sup>1</sup> H)	16	1
<sup>1</sup> H, <sup>15</sup> N NOESY	232	48	2048	14/4.7 ( <sup>1</sup> H)	40/117 ( <sup>15</sup> N)	14/4.7 ( <sup>1</sup> H)	16	1
<sup>1</sup> H, <sup>13</sup> C NOESY aliphatic	192	64	1024	14/4.7 ( <sup>1</sup> H)	80/39 ( <sup>13</sup> C)	14/4.7 ( <sup>1</sup> H)	8	1
<sup>1</sup> H, <sup>13</sup> C NOESY aromatic	144	32	2048	14/4.7 ( <sup>1</sup> H)	39/127 ( <sup>13</sup> C)	14/4.7 ( <sup>1</sup> H)	8	1
<b>(b) RuV ADPr bound</b>								
<sup>1</sup> H, <sup>15</sup> N HSQC	256	2048		44/120 ( <sup>15</sup> N)	14/4.7 ( <sup>1</sup> H)		4	1
<sup>1</sup> H, <sup>13</sup> C HSQC	512	2048		160/80 ( <sup>13</sup> C)	14/4.7 ( <sup>1</sup> H)		32	1
CBCANH	96	40	1024	72/39 ( <sup>13</sup> C)	44/117 ( <sup>15</sup> N)	14/4.7 ( <sup>1</sup> H)	32	1
CBCA(CO)NH	96	40	1024	72/39 ( <sup>13</sup> C)	44/117 ( <sup>15</sup> N)	14/4.7 ( <sup>1</sup> H)	32	1
HNCA	80	40	1024	42/55 ( <sup>13</sup> C)	44/117 ( <sup>15</sup> N)	14/4.7 ( <sup>1</sup> H)	8	1
HN(CO)CA	80	40	1024	42/55 ( <sup>13</sup> C)	44/117 ( <sup>15</sup> N)	14/4.7 ( <sup>1</sup> H)	16	1
HNCO	64	40	1024	18/175 ( <sup>13</sup> C)	44/117 ( <sup>15</sup> N)	14/4.7 ( <sup>1</sup> H)	8	1
HN(CA)CO	64	40	1024	18/175 ( <sup>13</sup> C)	44/117 ( <sup>15</sup> N)	14/4.7 ( <sup>1</sup> H)	8	1
HNHA	48	96	1024	44/120 ( <sup>15</sup> N)	14/4.7 ( <sup>1</sup> H)	14/4.7 ( <sup>1</sup> H)	16	1
HBHA(CBCACO)NH	112	40	1024	8/4.7 ( <sup>1</sup> H)	44/117 ( <sup>15</sup> N)	14/4.7 ( <sup>1</sup> H)	16	1
(H)CCH-TOCSY	128	48	1024	80/39 ( <sup>13</sup> C)	80/39 ( <sup>13</sup> C)	14/4.7 ( <sup>1</sup> H)	16	1
<sup>1</sup> H, <sup>15</sup> N NOESY	232	48	2048	14/4.7 ( <sup>1</sup> H)	44/120 ( <sup>15</sup> N)	14/4.7 ( <sup>1</sup> H)	8	1
<sup>1</sup> H, <sup>13</sup> C NOESY aliphatic	192	64	1024	14/4.7 ( <sup>1</sup> H)	80/39 ( <sup>13</sup> C)	14/4.7 ( <sup>1</sup> H)	8	1
<sup>1</sup> H, <sup>13</sup> C NOESY aromatic	144	32	2048	14/4.7 ( <sup>1</sup> H)	39/127 ( <sup>13</sup> C)	14/4.7 ( <sup>1</sup> H)	8	1

## Figure legends

**Fig. 1.** Sequence alignment of MDs of three viral families, *Matonaviridae* (RuV), *Coronaviridae* (SARS-CoV-2, SARS-CoV and MERS-CoV) and *Togaviridae* (CHIKV, VEEV and MAYV). Amino acid numbering is according to the native sequence of the multi-domain p150 for RuV MD and non-structural protein 3 (nsP3) for the rest. White color indicates non-conserved residues, light blue less conserved residues and dark blue conserved residues through all MDs.

**Fig. 2.** 2D  $^1\text{H}$ ,  $^{15}\text{N}$  HSQC assigned spectrum of the (a) 0.82 mM  $^{15}\text{N}$ ,  $^{13}\text{C}$  RuV MD in the free state and (b) 0.62 mM  $^{15}\text{N}$ ,  $^{13}\text{C}$  RuV MD in the presence of ADPr (molar ratio RuV MD:ADPr - 1:5) obtained at 298 K. The reported amino acids for RuV MD are numbered in accordance with the native sequence of the multi-domain p150 protein. The resonances corresponding to Asn and Trp side-chains are labeled with “sc”. The assigned residues arising from cloning artifacts are labeled with asterisks. The unassigned peaks of the spectra correspond to unassigned residues.

**Fig. 3.** Illustration of the unassigned residues in  $^1\text{H}$ ,  $^{15}\text{N}$  HSQC spectrum for the two RuV MD forms. (a) Cartoon representation of RuV MD structure in the free state (PDB ID: 8POC) and (b) ADPr bound (PDB ID: 8POE) (Stoll *et al.*, 2024) with missing residues colored in turquoise.

**Fig. 4.** Secondary structure and flexibility analysis of RuV MD in (a) apo and (b) ADPr bound state. Comparison of secondary structure analysis from the crystal structures (upper; 8POC and 8POE, respectively) with secondary structure prediction based on NMR experimental data using the TALOS+ server (Shen *et al.*, 2009) (middle) shows good agreement for both RuV MD forms. Red cartoon indicates  $\alpha$ -helix and blue arrow  $\beta$ -strand. In the plot (lower), the  $\alpha$ -helix and  $\beta$ -strands SS values predicted using the TALOS+ server for each residue are shown as positive and negative values, respectively. The negative SS values for  $\beta$ -strands propensities are given for illustration purposes. Values close to 1 or -1 indicate high possibility for  $\alpha$ -helix and  $\beta$ -strands, respectively. The flexibility of RuV MD is also depicted as Random Coil Index (RCI) derived  $S^2$  (RCI- $S^2$ ) values predicted by TALOS+ server (Shen *et al.*, 2009) and shown with blue dots. The reported amino acids for RuV MD are numbered in accordance with the native sequence of the multi-domain p150 protein.

# Figures

## Fig. 1.

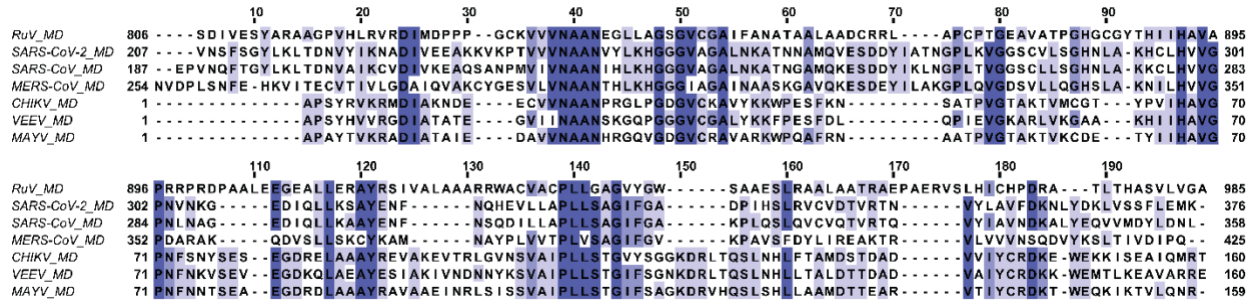
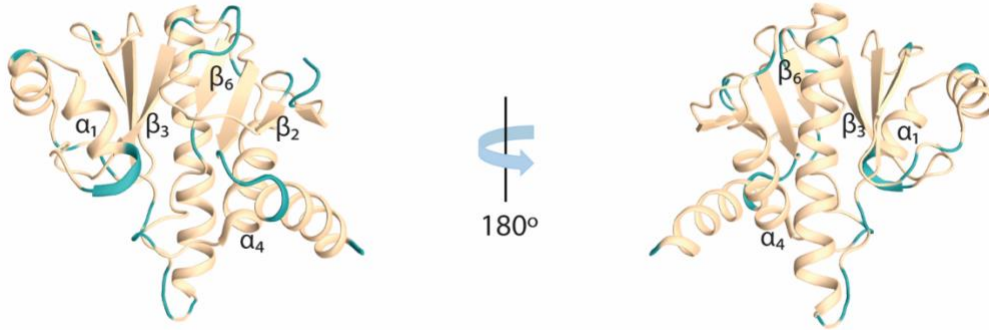




**Fig. 3.**

**a**



**b**

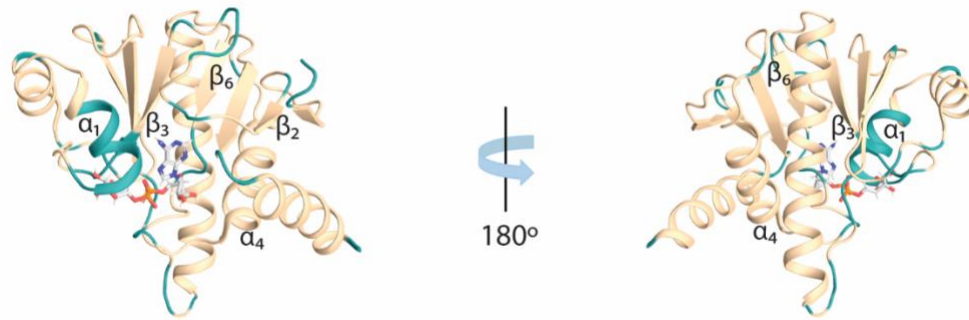


Fig. 4.

